TUDelft

Delft University of Technology

Demonstration of Eu^{3+} → Eu^{2+} Energy Transfer in NIR Emitting CaO:Eu^{2+},Eu^{3+} LED Phosphor and its Implication for the Role of Eu^{3+} as a Killer Center for Long Wavelength Eu^{2+} Emission

van Aarle, Casper; Ingham, Robert; van der Heijden, Clara; Budwilowitz, Koray; Niehe, Meesz; Dugulan, Iulian; Hintzen, Hubertus T.

Important note
To cite this publication, please use the final published version (if applicable).
Please check the document version above.

Demonstration of Eu^{3+} → Eu^{2+} Energy Transfer in NIR Emitting CaO:Eu^{2+},Eu^{3+} LED Phosphor and its Implication for the Role of Eu^{3+} as a Killer Center for Long Wavelength Eu^{2+} Emission

Casper van Aarle,* Robert Ingham, Clara van der Heijden, Koray Budwilowitz, Meesz Niehe, Iulian Dugulan, and Hubertus T. Hintzen

While Eu^{2+} → Eu^{3+} energy transfer is well known, in this study the energy transfer from Eu^{3+} to Eu^{2+} is reported for the first time. The predominant condition for Eu^{3+} → Eu^{2+} energy transfer is a Eu^{2+} 4f^{6}5d band at lower energy than the position of the Eu^{3+} 4f^6[^{5}D$_0$] level, which is fulfilled in Eu-doped CaO. X-ray powder diffraction, Eu Mössbauer spectroscopy and optical absorption measurements are employed to determine the Eu^{3+} and Eu^{2+} concentrations in the prepared CaO:1at.%Eu samples. Synthesis in an H$_2$/N$_2$ atmosphere and addition of graphite powder as a reducing agent to the starting mixture are found to result in respective Eu^{3+} and Eu^{2+} concentrations of 0.6–0.7% and 0.3–0.4%. For this sample, the Eu^{3+} → Eu^{2+} energy transfer efficiency is estimated to be high (> 90%). This is explained by the high oscillator strength of the 4f^7 → 4f^{6}5d excitation transition of the Eu^{2+} ion to which energy is transferred. As the Eu^{2+} 4f^{6}5d band lies below the Eu^{3+} 4f^6[^{5}D$_0$] level, Eu^{3+} does not act as a killer center for the near-infrared (NIR) Eu^{2+} emission at about 720 nm. Therefore, a full reduction of Eu^{3+} is not required to attain a high quantum efficiency. Implications of the demonstrated Eu^{3+} → Eu^{2+} energy transfer for application of long wavelength Eu^{2+} phosphors are discussed.

1. Introduction

Eu is an important luminescent center for lighting and display applications, either in the divalent (Eu^{2+}) or in the trivalent (Eu^{3+})

state. The Eu^{3+} ion shows 4f^6-4f^6 (mainly ^{5}D$_0$ → ^{7}F$_J$) line emissions at fixed wavelengths in the red part of the spectrum independent of the host lattice, while the ratio of the ^{5}D$_0$ → ^{7}F$_1$ / ^{5}D$_0$ → ^{7}F$_2$ emissions is influenced by the presence of inversion symmetry at the Eu^{3+} center.[1] On the contrary, the Eu^{2+} ion gives a 4f^{6}5d → 4f^7 band emission with a peak maximum strongly dependent on the local coordination of Eu^{2+} in the host lattice, which can shift from ultraviolet (UV) to the infrared (IR) part of the spectrum.[2,3]

Eu^{3+}-doped Y$_2$O$_2$S was already used as red-emitting material in classical cathode-ray (television) tubes before the characteristics of Eu^{2+}- and Eu^{3+}-activated phosphors enabled the development of the tricolor tube fluorescent lamp in the 70s of last century as a next-generation lighting device. By mixing three phosphors emitting in the blue, green and red part of the spectrum according to the requirement predicted by simulations, an optimum combination of a high color rendering index with a high lumen efficiency could be achieved, outperforming the conventional fluorescent tube lamp-based on mixing of blue and yellow light of Sb^{3+},Mn^{2+}-doped halo-phosphate phosphor. The blue-emitting phosphor in the tricolor fluorescent lamp was a Eu^{2+}-doped aluminate phosphor with beta-alumina structure (BaMgAl$_{10}$O$_{17}$:Eu^{2+}), whereas a simple Eu^{3+}-doped oxide phosphor (Y$_2$O$_3$:Eu^{3+}) was used as the red-emitting component in combination with CeMgAl$_{11}$O$_{19}$:Tb as the green-emitting material.[4]

Since the invention of efficient UV-blue emitting (Ga,In)N light-emitting diodes (LEDs) by Physics Nobel prize winner Nakamura in 1993, it became possible to design white light emitting devices with higher efficiency and longer life-time. The first white light LEDs were obtained by combining the blue-emitting LED with a phosphor which absorbs part of the blue LED light and converts it into yellow light, similar to the concept of mixing blue and yellow light of Sb^{3+},Mn^{2+}-doped halo-phosphate phosphor in the first fluorescent lamps. The already known

C. van Aarle, R. Ingham, C. van der Heijden, K. Budwilowitz, M. Niehe, I. Dugulan, H. T. Hintzen
Faculty of Applied Sciences
Delft University of Technology
Mekelweg 15, Delft 2629 JB, The Netherlands
E-mail: c.vanaarle@tudelft.nl

**ADVANCED
SCIENCE NEWS**

www.advancedsciencenews.com

**ADVANCED
OPTICAL
MATERIALS**

www.advopticalmat.de

yellow-emitting phosphor $Y_3Al_5O_{12}$:Ce^{3+} (YAG:Ce) is well suited as a blue-yellow conversion phosphor and still in use for this purpose. In a later stage improved white light LEDs were developed by applying phosphors converting the UV LED radiation into a combination of blue, green and red light, similar to the concept on which the tricolor lamp is based.

In the meantime, a wide variety of blue-, green- and red-emitting phosphors have been proposed, developed and commercialized, of which many based on Eu^{2+}-doped materials.[5] Red Eu^{2+} emission is usually found for covalent host lattices with strong nephelauxetic effect and strong crystal field (sulfides, nitrides), while blue and green emission is obtained for all kinds of host lattices with a rather weak nephelauxetic effect and weak crystal field (phosphates, silicates, aluminates, borates). Examples of red-emitting Eu^{2+}-activated phosphors are given by the Eu^{2+}-doped sulfides such as CaS:Eu^{2+} and SrS:Eu^{2+}, and the Eu^{2+}-doped nitrides such as $Sr_2Si_5N_8$:Eu^{2+} and CaAlSiN$_3$:Eu^{2+}. Because the nitride phosphors are chemically more stable than the sulfide phosphors and moreover show less thermal quenching of the luminescence, they are commercialized for application in white light LEDs.

A further shift of the Eu^{2+} emission beyond visible red emission to longer wavelengths for lattices with still stronger nephelauxetic effect and/or higher crystal field strength makes it useless for application in white light LEDs for lighting or display applications, because of the decreased eye sensitivity and consequently lower luminous efficacy. At the same time, such long wavelength IR Eu^{2+} emission has recently become of interest for application in near-infrared (NIR) LEDs for use in the fields of biomedical imaging, remote sensing, security monitoring, agricultural lighting, etc.[6]

However, compared to red Eu^{2+} band emission for white light LEDs, red line emission originating from Eu^{3+} has the advantage of avoiding lumen losses for emissions at too high wavelengths, and therefore is of potential benefit when the Eu^{3+} $^5D_0 \rightarrow {}^7F_4$ emission at about 700 nm is not too intense. On the other hand, the challenge with the Eu^{3+} ion is obtaining sufficient absorption of radiation emitted by the UV-blue pump LEDs. For application of the well-known red-emitting Y_2O_3:Eu^{3+} phosphor in tricolor fluorescent lamps, the Eu^{3+} ion is excited in the Eu^{3+} $\leftarrow O^{2-}$ charge transfer band whose position well matches with the 254 nm line of the mercury gas discharge. Because the Eu^{3+}-ligand charge transfer band cannot be shifted to lower energies overlapping with the emission of UV-blue pump LEDs (370–450 nm), the Eu^{3+} ion would not be efficiently excited in this way.

As an alternative approach the absorption by $4f^6$-$4f^6$ transitions ($^7F_0 \rightarrow {}^5L_6$ excitation) at about 400 nm has been proposed for Eu^{3+}-doped materials, e.g. $Ca_3La(GaO)_3(BO_3)_4$:Eu^{3+}.[7] However, the absorption remains quite weak despite a high Eu^{3+} concentration which moreover may cause concentration quenching of the luminescence. Therefore this approach does not seem viable and the best way out is sensitization of the Eu^{3+} luminescence by co-doping with e.g. VO_4^{3-}, WO_4^{2-}, Ce^{3+}, or Eu^{2+}. More recently, effective sensitization of Eu^{3+} by Tb^{3+}-co-doping has been claimed for $Li_3Ba_2La_3(MoO_4)_8$:Eu^{3+},Tb^{3+}, and the Eu^{3+} excitation probability was effectively increased more than an order of magnitude by 1) proper host-lattice selection, 2) increased sensitization by co-doping, 3) optical interaction with other down-converters for increased excitation at wave-

lengths outside the blue regime, and 4) geometrical factors.[8] Quenching of the luminescence may be caused by intervalence charge transfer (Ce^{4+}/Tb^{4+}-Eu^{2+}) transitions, which can be reduced by interparticle energy transfer when mixing nanoparticles of LaPO$_4$:Tb/LaPO$_4$:Eu and LaPO$_4$:Tb/Y(V,P)O$_4$:Eu.[9]

Energy transfer from Eu^{2+} to Eu^{3+} has been demonstrated for several mixed valency Eu-doped phosphors, such as YF_3:Eu^{2+},Eu^{3+}[10] and $CaAl_2Si_2O_8$:Eu^{2+},Eu^{3+}.[11] The energy of the Eu^{2+} $4f^65d$ band has to be higher than that of the Eu^{3+} emitting $4f^6[^5D_0]$ level, enabling $4f^6[^7F_0] \rightarrow 4f^6[^5D_0]$ excitation of Eu^{3+}.

In case of incomplete or inefficient $Eu^{2+} \rightarrow Eu^{3+}$ energy transfer, the Eu^{2+} emission can be combined with red Eu^{3+} emission in a single phosphor. In this way for a blue-green Eu^{2+} emission (at 490–500 nm) a white light-emitting phosphor can be created, analogous to the first white light fluorescent lamp phosphor based on a halo-phosphate host lattice co-doped with Sb^{3+} (blue light) and Mn^{2+} (yellow light). Some examples of Eu^{2+}/Eu^{3+}-co-doped white light emitting phosphors are $MgSrLa_8(SiO_4)_6O_2$:Eu^{2+},Eu^{3+}[12] and $Na_5Al(PO_4)_2F_2$:Eu^{2+},Eu^{3+}.[13] Luminescent materials showing a combination of Eu^{2+} and Eu^{3+} emission, as influenced by the temperature, have become of interest as thermosensitive phosphors for application in the field of remote temperature sensing.[14]

As already mentioned, in case of a very high nephelauxetic effect (i.e., covalent lattice) and a strong crystal field (i.e., small site coordinated by highly charged anions), the Eu^{2+} emission will shift to the near-infrared (NIR) part of the spectrum. Consequently, the Eu^{2+} $4f^65d$ level is at too low energy for transferring energy to Eu^{3+}. Now, the most intense Eu^{3+} $4f^6[^5D_0] \rightarrow 4f^6[^7F_J]$ transitions overlap with the Eu^{2+} $4f^7 \rightarrow 4f^65d$ excitation bands. In this case, the reverse energy transfer from Eu^{3+} to Eu^{2+} would be expected according to the theories on energy transfer developed by Förster and Dexter.[15,16] However, so far, such $Eu^{3+} \rightarrow Eu^{2+}$ energy transfer has never been reported.

The series of MO (M = Mg, Ca, Sr, Ba) compounds with rocksalt structure enables the variation of the crystal field strength by changing M with different ionic radius, and therefore MO is an ideal model system for studying the influence of M on the Eu^{2+} $4f^65d$ crystal field splitting, the co-existence of Eu^{2+} and Eu^{3+} and energy transfer phenomena between them. Eu(II)O is also stable with a rocksalt structure and can form solid solutions with MO. In MO with rocksalt structure M is octahedrally coordinated with six O^{2-} anions with inversion symmetry. For octahedral coordination with inversion (O_h) symmetry the Eu^{2+} $4f^65d$ band is split into an e_g and t_{2g} level, while the Eu^{3+} ion can be used as a probe for checking the absence or presence of local inversion symmetry due to local distortions.

For studying whether or not $Eu^{3+} \rightarrow Eu^{2+}$ energy transfer occurs, in this work we have chosen for CaO:Eu. Literature data confirm that the similar size of Ca^{2+} and Eu^{3+} allows for the co-existence of Eu^{2+} and Eu^{3+} in the CaO host lattice, and show that the peak wavelength of the Eu^{2+} band emission is at about 720 nm.[17] The ionic radius of Ca^{2+} is smaller than that of Eu^{2+}, inducing a high crystal field strength, and consequently a large downward shift of the lowest $4f^65d(t_{2g})$ level. Because of the long emission wavelength of Eu^{2+} in CaO (i.e., low energy of the lowest level Eu^{2+} $4f^65d$ band), energy transfer from Eu^{2+} to Eu^{3+} is no longer possible. Here we will report for the first time

**ADVANCED
SCIENCE NEWS**

www.advancedsciencenews.com

**ADVANCED
OPTICAL
MATERIALS**

www.advopticalmat.de

that energy transfer from Eu^{3+} to Eu^{2+} takes place as verified in $CaO:Eu^{2+},Eu^{3+}$.

While CaO:Eu is a suitable model compound for studying Eu^{3+} → Eu^{2+} energy transfer, there has also been an emerging interest in CaO:Eu as phosphor for LED applications. Recently, Qiao et al. reported an internal quantum efficiency of about 76% on a CaO:Eu sample showing exclusively Eu^{2+} emission at about 740 nm,[18] in agreement with the results of Yamashita.[17] CaO:Eu prepared with a special synthesis technique that was used to construct a high-power NIR LED device with record performance.[18] However, Zhao et al.[19] and Hao et al.[20] reported Eu^{2+} emission bands at shorter wavelengths (about 661 and 460 nm, respectively) for CaO:Eu samples prepared in different ways, enables the use as red-,[19] respectively blue-emitting phosphor[20] in white LEDs.

In this work, a number of Eu-doped CaO samples were prepared with a solid state synthesis method in air versus making use of various reducing agents (H_2, Ca_3N_2, C). The Eu-concentration was 1.0 at.%. The Eu^{2+} and Eu^{3+} concentrations can be measured apart from each other by several techniques, e.g. XPS,[21,22] XANES,[23,24] magnetic measurements[25] or Eu Mössbauer spectroscopy.[26] In this work, we have selected the last technique because of its availability at our institute and the possibility to measure the relative bulk concentrations of Eu^{2+} and Eu^{3+} in a straightforward way. Moreover, information can be obtained about site occupancies and bonding characteristics. Eu Mössbauer spectroscopy has previously been used for the characterization of the commercial phosphors $Y_2O_3:Eu^{3+}$[27] and $BaMgAl_{10}O_{17}:Eu^{2+}$,[28] while relative Eu^{2+}/Eu^{3+} concentrations have been determined for $SrAl_{12}O_{19}:Eu^{2+},Eu^{3+}$.[29] As the main result of this paper the occurrence of Eu^{3+} → Eu^{2+} energy transfer in $CaO:Eu^{2+},Eu^{3+}$ will be demonstrated by emission, excitation, and time-resolved luminescence measurements. In addition, the implication for its role of Eu^{3+} as a killer center for the Eu^{2+} emission will be discussed.

2. Results

To see whether the synthesis yielded single phase reaction products, **Figure 1a–c** shows the powder X-ray diffractograms of the three CaO:1at.%Eu samples. For comparison, the ICDD reference patterns for CaO and Eu_2O_3 are shown in Figure 1d,e, respectively. For CaO:1at.%Eu (air) in Figure 1a, very low-intensity diffraction peaks are observed that cannot be ascribed to the CaO phase. These diffraction peaks are marked with arrows that correspond with Eu_2O_3 and are therefore ascribed to Eu_2O_3 left over from the starting materials, possibly due to the low solubility of Eu^{3+} in CaO at the used firing temperature. A similar incomplete incorporation of Eu_2O_3 was observed by Zhao et al. when doping CaO with 2 mol.% Eu_2O_3.[37] All peaks in Figure 1b,c can be ascribed to the cubic CaO phase, no second phases are observed. Apparently, synthesis under reducing conditions helps with incorporation of Eu, as the solubility of Eu^{2+} is most likely higher than that of Eu^{3+} owing to Eu(II)O having the same rock salt crystal structure as CaO.

To determine the precision with which the lattice parameter a can be measured, **Figure 2a** shows a plot of a calculated for each diffraction peak of the Si internal standard versus $f(\theta)$ (see Equation 6). The true lattice parameters of the Si internal standard as
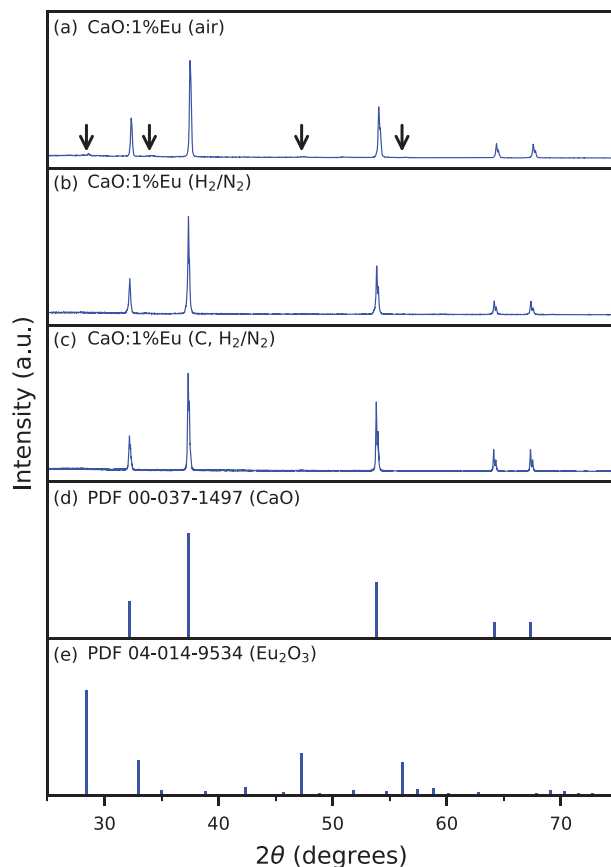
Figure 1. X-ray diffractograms of a) CaO:1at.%Eu (air), b) CaO:1at.%Eu (H_2/N_2), and c) CaO:1at.%Eu (C, H_2/N_2). ICDD reference patterns d) CaO (PDF 00-037-1497), and e) Eu_2O_3 (PDF 04-014-9534).
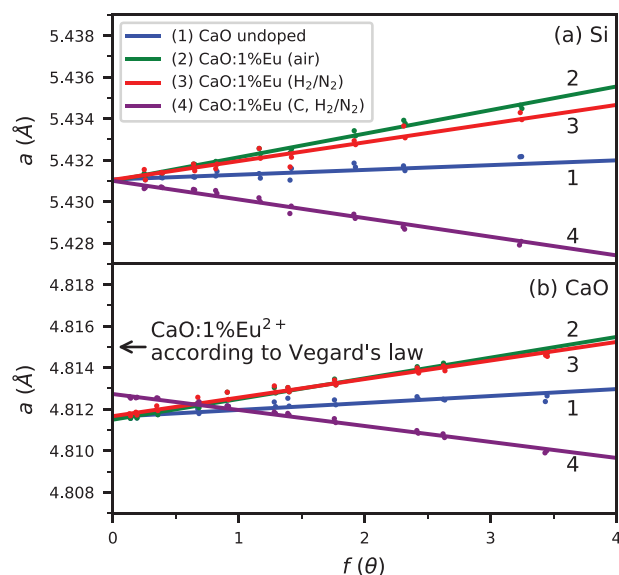

Figure 2. Lattice parameter a as a function of $f(\theta)$ for a) Si internal standard and b) CaO samples. The real lattice parameter is found at $f(\theta) = 0$.

Table 1. Lattice parameters of the internal standard Si (a_{Si}) and the CaO samples (a_{CaO}) determined by extrapolating the fits with Equation (6) in Figure 2 to $f(\theta) = 0$. Eu^{2+} and Eu^{3+} concentrations are estimated from lattice parameters (see text).

Sample	a_{Si}	a_{CaO}	at.% Eu^{3+}	at.% Eu^{2+}
CaO undoped	5.4311	4.8116	0	0
CaO:1at.%Eu (air)	5.4310	4.8115	1	0
CaO:1at.%Eu (H_2/N_2)	5.4311	4.8117	1	0
CaO:1at.%Eu (C, H_2/N_2)	5.4310	4.8127	0.7	0.3

determined for $f(\theta) = 0$ are shown in **Table 1**. Despite linear dependencies of a on $f(\theta)$ with different slopes, the intercept value is almost the same showing internal consistency. A value of $a = 5.431\pm0.001$ Å is found, which corresponds well to the value of 5.43159 Å specified by the National Institute of Standards and Technology.[38] The minor spread in the lattice parameter determined for Si shows that variations in a of CaO larger than 0.001 Å can be interpreted as real physical effects.

Figure 2b shows the lattice parameter a versus $f(\theta)$ for the CaO samples. As opposed to the Si internal standard in Figure 2a, a for CaO does not converge to the same value for all samples. Again, the true lattice parameters are shown in Table 1. The effect of doping with 1 at.%Eu for the CaO:1at.%Eu (air) and CaO:1at.%Eu (H_2/N_2) samples is not apparent as they vary by only 0.0001 Å from the undoped CaO sample. As CaO:1at.%Eu (air) is expected to contain exclusively Eu^{3+}, it can be concluded that incorporation of minor amounts of Eu^{3+} has negligible effect on a.

The change in a for CaO:1at.%Eu (C, H_2/N_2) is an order of magnitude larger than for the other samples (0.001 Å vs 0.0001 Å). As CaO and Eu(II)O both crystallize in the rock salt structure, the lattice parameter expected for CaO:1at.%Eu^{2+} can be calculated using Vegard's law. Using $a = 4.8116$ Å for undoped CaO (Table 1) and $a = 5.142$ Å for Eu(II)O,[39] it is calculated that $a = 4.815$ Å for CaO:1at.%Eu^{2+} ($Ca_{0.99}Eu_{0.01}O$). This value is indicated in Figure 2 by the arrow. CaO:1at.%Eu (C, H_2/N_2) shows about 30% of the increase in a versus undoped CaO compared to what is expected for CaO:1at.%Eu^{2+}. When assuming the effects of Eu^{3+} on a are negligible, the Eu^{2+} concentration can be estimated to be about 0.3 at.% in this sample and consequently, the Eu^{3+} concentration is about 0.7 at.%.

Figure 3 shows the Kubelka–Munk absorption spectra of all three CaO:1at.%Eu samples in the 420–800 nm range. CaO:1at.%Eu (air) shows no increased absorption compared to the undoped CaO reference. This indicates that this samples contains exclusively Eu^{3+}, as the absorption strength of the parity forbidden Eu^{3+} $4f^6 \rightarrow 4f^6$ transitions is too low to be observable in the figure. CaO:1at.%Eu (H_2/N_2) shows an absorption band that corresponds well with the Eu^{2+} $4f^7 \rightarrow 4f^65d(t_{2g})$ absorption band reported in literature for CaO: Eu^{2+}, Eu^{3+}.[17] This shows that the sample contains some Eu^{2+}, even though no lattice expansion was observed with XRD (Table 1). CaO:1at.%Eu (C, $H_2/.N_2$) shows stronger absorption from the $4f^7 \rightarrow 4f^65d(t_{2g})$ band compared to CaO:1at.%Eu (H_2/N_2), confirming its higher Eu^{2+} concentration as shown with XRD (Table 1). Based on the Kubelka–Munk absorption of CaO:1at.%Eu (H_2/N_2) compared to that of CaO:1at.%Eu (C,H_2/N_2), it is estimated that the Eu^{2+} concentration is approximately 0.1 at.% in CaO:1at.%Eu (H_2/N_2).
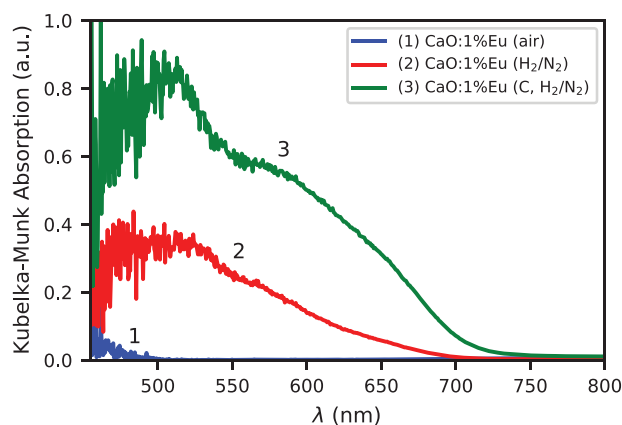
Figure 3. Kubelka–Munk absorption spectra of CaO:1at.%Eu prepared with three different synthesis methods using undoped CaO as reference sample.

The presence of Eu^{2+} has been directly demonstrated using Eu Mössbauer spectroscopy. Using a $^{151}SmF_3$ source and a EuF_3 reference sample, Eu^{3+} creates an absorption line around 0 mm s^{-1}, while the signal of Eu^{2+} is typically positioned around −13 mm s^{-1}.[26] **Figure 4a,b** shows the Mössbauer spectra for CaO:1at.%Eu (air) and CaO:1at.%Eu (H_2/N_2), respectively. They both contain a single absorption line around 1 mm s^{-1}, no absorption around −13 mm s^{-1} was observed. This indicates that the samples contain primarily Eu^{3+}. The data was fitted with a single Lorentzian function, its fit parameters are provided in **Table 2**. The isomer shift
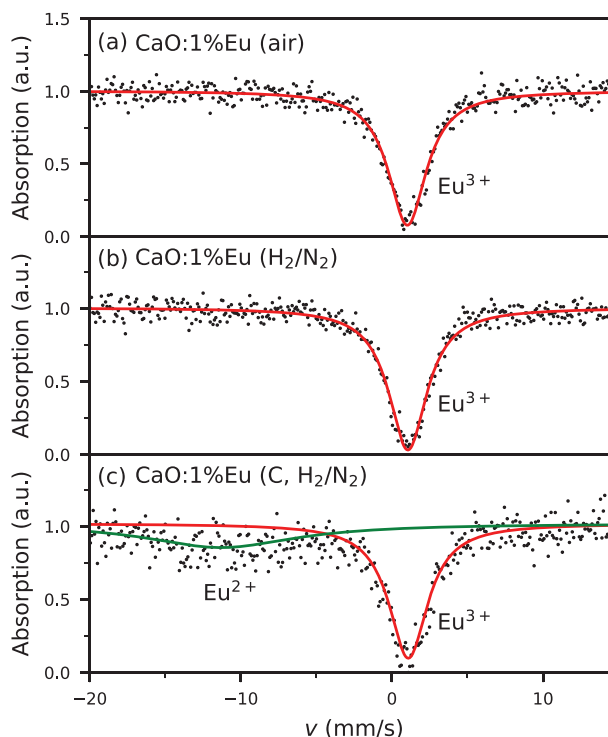
Figure 4. ^{151}Eu Mössbauer spectra of a) CaO:1at.%Eu (air), b) CaO:1at.%Eu (H_2/N_2), and c) CaO:1at.%Eu (C, H_2/N_2). The signal at −13 mm s^{-1} for CaO:1at.%Eu (C,H_2/N_2) shows the presence of Eu^{2+}.

**ADVANCED
SCIENCE NEWS**

www.advancedsciencenews.com

**ADVANCED
OPTICAL
MATERIALS**

www.advopticalmat.de

Table 2. Mössbauer fit parameters for the Eu-doped CaO samples. δ denotes the isomer shift and Γ denotes the linewidth.

| Sample	ion	δ [mm s^{-1}]	Γ [mm s^{-1}]	at.%
CaO:1at.%Eu (air)	Eu^{3+}	1.02±0.02	3.06±0.07	1
	Eu^{2+}	—	—	0
CaO:1at.%Eu (H$_2$/N$_2$)	Eu^{3+}	1.05±0.02	3.08±0.07	1
	Eu^{2+}	—	—	0
CaO:1at.%Eu (C, H$_2$/N$_2$)	Eu^{3+}	1.08±0.04	3.12±0.13	0.6
	Eu^{2+}	−11.31±0.46	12.13±1.89	0.4

is a measure of the 6s-electron density at the Eu nucleus, which becomes higher for decreasing Eu-O distance and increasing covalency, while the line width gets larger for asymmetric and more Eu^{3+} centers. The isomer shift of 1.0–1.1 mm s^{-1} is similar to that observed for other oxide compounds,[26] such as Y$_2$O$_3$:Eu^{3+},[27] and considerably higher than that of the EuF$_3$ reference compound because of the increased covalent character of CaO. The linewidth higher than 3 mm s^{-1} is very large,[40] ascribed to the presence of more Eu^{3+} centres in CaO:Eu[41] with somewhat different isomer shift and linewidth values.

In Figure 4c, the Mössbauer spectrum of CaO:1at.%Eu (C, H$_2$/N$_2$) is shown. In addition to the Eu^{3+} absorption line around 1 mm s^{-1} is, it also shows a line at about −11.3 mm s^{-1}, indicating that the sample contains a significant amount of Eu^{2+}. The data has been fitted using two Lorentzian functions, of which the fitting parameters are also provided in Table 2. The Eu^{3+} isomer shift is somewhat higher than for the CaO:1at.%Eu (air) and CaO:1at.%Eu (H$_2$/N$_2$) compounds, while from the slightly larger lattice parameter $\langle a\rangle$ a lower value is expected.[27] This indicates an increased covalency,[42] which is caused by the presence of Eu^{2+} in the sample. Some disorder seems to be introduced as well, resulting in a larger linewidth, and both effects suggest that Eu^{2+} and Eu^{3+} are quite close to each other in the CaO host lattice.

The Eu^{2+} isomer shift of about −11.3 mm s^{-1} is among the highest (i.e., least negative) values reported[26] and in the range of covalent compounds such as sulfides (isomer shift CaS:Eu = −11.5 mm s^{-1};[43] EuS = −11.7 mm s)$^{-1}$[44] and nitrides (isomer shift Eu$_2$SiN$_3$ = −10.66 mm s^{-1};[45] Eu$_2$Si$_5$N$_8$ = −11.88 mm s^{-1};[46] Eu$_3$(BN$_2$)$_2$ = −11.4 mm s^{-1}, Eu$_{0.937}$Ba$_8$(BN$_2$)$_6$ = −10.7 mm s^{-1}).[47] The Eu^{2+} signal with a linewidth of about 12.1 mm s^{-1} (Table 2) is very broad as compared with other Eu^{2+}-activated phosphors.[29] For SrAl$_{12}$O$_{19}$:Eu with magnetoplumbite structure the linewidth increases from 3.6 mm s^{-1} for 100% Eu (90% Eu^{2+}) to 11.0 mm s^{-1} for 5% Eu (4.5% Eu^{2+}), which is ascribed to paramagnetic relaxation effects.[29] Only a minor increase of the Eu^{2+} linewidth to 12.1 mm s^{-1} for more than a factor 10 lower Eu^{2+} concentration in CaO:1at.%Eu (0.3–0.4% Eu^{2+}) is most probably due to the high symmetric Ca^{2+} site with inversion symmetry on which Eu^{2+} is incorporated in CaO, reducing the linewidth of the Eu^{2+} Mössbauer signal. Due to further broadening of the Eu^{2+} signal for lower Eu^{2+} concentrations present in the sample CaO:1at.%Eu prepared in H$_2$/N$_2$ atmosphere the detection of Eu^{2+} with Mössbauer spectroscopy was impossible for the used measurement conditions.

Under the assumption that Eu^{2+} and Eu^{3+} have the same recoil-free fraction, the Eu^{2+} and Eu^{3+} concentrations can be esti-

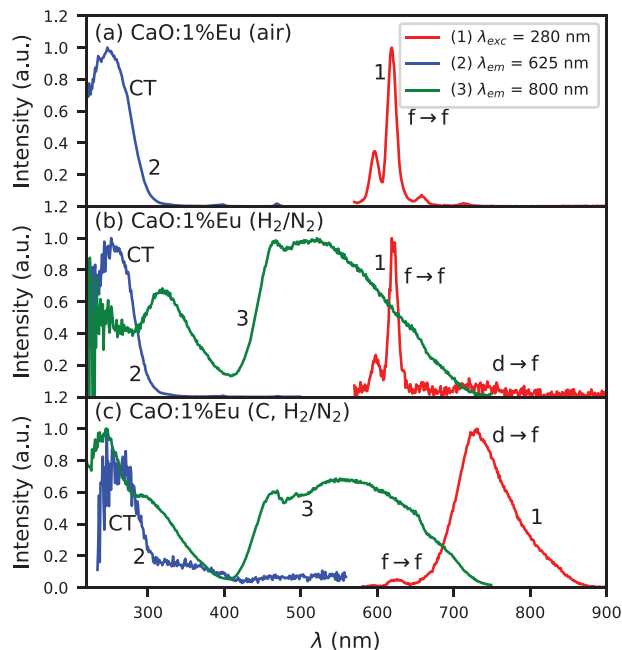**Figure 5.** Photoluminescence excitation and emission spectra of a) CaO:1at.%Eu (air), b) CaO:1at.%Eu (H$_2$/N$_2$), and c) CaO:1at.%Eu (C, H$_2$/N$_2$).

mated from the ratio between the area under the absorption lines. For CaO:1at.%Eu (C, H$_2$/N$_2$), this yields Eu^{2+} and Eu^{3+} concentrations of about 0.4% and 0.6%, respectively, which is close to the concentrations determined with XRD (Table 1). For CaO:1at.%Eu (H$_2$/N$_2$), the absence of a Eu^{2+} absorption line makes it impossible to estimate the relative concentrations in this sample. However, considering the argumentation before, the fact that the Eu^{3+} Mössbauer isomer shift and linewidth are in between those of the CaO:1at.%Eu (air) and CaO:1at.%Eu (C, H$_2$/N$_2$) samples is consistent with the presence of some Eu^{2+} in the CaO:1at.%Eu (H$_2$/N$_2$) sample.

Figure 5a shows the photoluminescence excitation and emission spectra of CaO:1at.%Eu (air). When excited at 280 nm, the emission spectrum (Curve 1) shows exclusively Eu^{3+} emission due to the 4f^6[^{5}D$_0$] → 4f^6[^{7}F$_J$] transitions. From the 4f^6[^{5}D$_0$] → 4f^6[^{7}F$_2$] emission (at about 625 nm) being stronger than the 4f^6[^{5}D$_0$] → 4f^6[^{7}F$_1$] emission (in the range 590–595 nm) it can be concluded that the inversion symmetry at the Ca^{2+} site is lifted,[1] evidently as a consequence of the necessity of charge compensation if Eu^{3+} is replacing Ca^{2+}. The excitation spectrum when monitoring the Eu^{3+} line emission at 625 nm (Curve 2) shows a broad band centered at 250 nm which is ascribed to the Eu^{3+} CT band.[17,19]

When exciting CaO:1at.%Eu (H$_2$/N$_2$) at 280 nm (Figure 5b), it shows primarily the same Eu^{3+} line emission as CaO:1at.%Eu (air). In addition a weak broad emission band is observed between 700 and 800 nm, which is assigned to the Eu^{2+} 4f^{6}5d → 4f^7 emission. The excitation spectrum when monitoring the Eu^{3+} emission at 625 nm (Curve 2) shows the same Eu^{3+} CT band as was observed for CaO:1at.%Eu (air). The excitation spectrum when monitoring the Eu^{2+} 4f^{6}5d → 4f^7 emission at 800 nm (Curve 3) contains the 4f^7 → 4f^{6}5d(t$_{2g}$) band between 400 and 750 nm and the 4f^7 → 4f^{6}5d(e$_g$) band between 200 and 400 nm.

ADVANCED
SCIENCE NEWS

www.advancedsciencenews.com

ADVANCED
OPTICAL
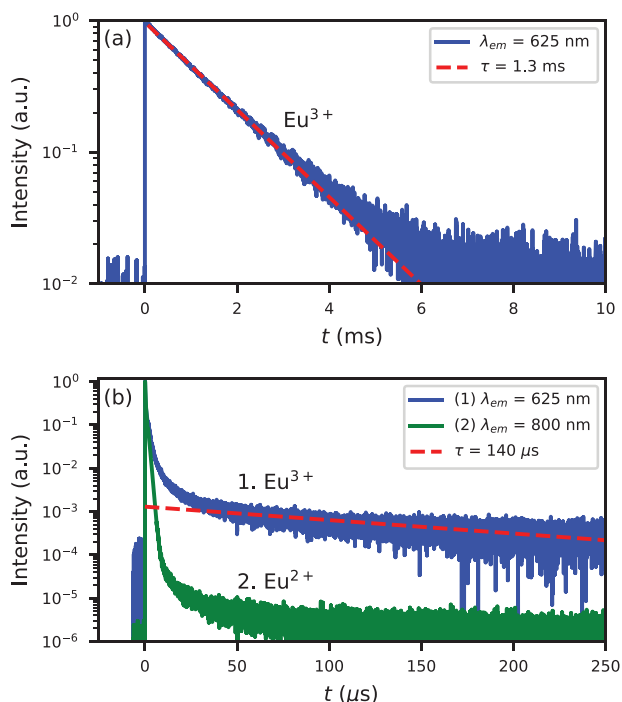**MATERIALS**

www.advopticalmat.de

Figure 6. Photoluminescence decay under 280 nm excitation. a) CaO:1at.%Eu (air) and b) CaO:1at.%Eu (C, H_2/N_2).

Between 200 and 300 nm, the excitation spectrum of the Eu^{2+} emission shows a dip where the Eu^{3+} CT band is at maximum. This is ascribed to competitive absorption between Eu^{2+} and Eu^{3+}.

Figure 5c shows the emission spectrum of CaO:1at.%Eu (C, H_2/N_2) under 280 nm excitation (Curve 1). It shows almost exclusively Eu^{2+} $4f^65d \rightarrow 4f^7$ broad band emission between 650 and 900 nm with top at 720 nm. The low intensity Eu^{3+} line emission can still be observed around 625 nm. The excitation spectrum when monitoring the Eu^{3+} emission at 625 nm (Curve 2) again shows the same Eu^{3+} CT band at about 250 nm. The excitation signal between 300 and 550 nm comes from the Eu^{2+} $4f^65d \rightarrow 4f^7$ emission slightly overlapping with the Eu^{3+} emission at 625 nm. The excitation spectrum when monitoring the Eu^{2+} $4f^65d \rightarrow 4f^7$ emission at 800 nm again contains the Eu^{2+} $4f^7 \rightarrow 4f^65d(t_{2g})$ and $4f^7 \rightarrow 4f^65d(e_g)$ bands. Compared to CaO:1at.%Eu (H_2/N_2), the excitation spectrum of the Eu^{2+} emission in CaO:1at.%Eu (C, H_2/N_2) shows an increase in intensity between 200 and 300 nm. This band was also observed by Yamashita in CaO:Eu^{2+},Eu^{3+} and was believed to be part of the Eu^{2+} $4f^7 \rightarrow 4f^65d(e_g)$ excitation band.[17] However, based on the results presented in this work, our presumption is that this band is the Eu^{3+} CT band as a result of energy transfer from Eu^{3+} to Eu^{2+}, superimposed on the Eu^{2+} $4f^7 \rightarrow 4f^65d(e_g)$ band.

The internal quantum efficiency of the CaO:1at.%Eu (C, H_2/N_2) sample was measured by exciting the sample at 470 nm in the $4f^7 \rightarrow 4f^65d(t_{2g})$ band and using undoped CaO as reference. This yielded a value of ≈20%.

Figure 6a shows the photoluminescence decay of CaO:1at.%Eu (air) after excitation in the Eu^{3+} CT band at 280 nm. The $4f^6[^5D_0] \rightarrow 4f^6[^7F_2]$ emission was monitored at 625 nm. The resulting de-

cay curve has a primary decay component of 1.3 ms, which originates from the Eu^{3+} center with shortest decay time reported in literature for CaO:Eu^{3+}.[17,41,48] The good correspondence with decay time values reported for CaO:Eu^{3+} in literature excludes that any significant influence comes from the left over Eu_2O_3 starting material found in this sample (Figure 1), specifically because this would produce a component with decay time of 170 μs or faster.[49,50] The decay time of 1.3 ms is typical for Eu^{3+} substituted on a non-centrosymmetric site,[51] as expected for destroying the inversion symmetry at the Ca^{2+} site as a consequence of charge compensation. The slight deviation from exponential decay at longer timescales is ascribed to slower decaying Eu^{3+} centers, e.g., Eu^{3+} on the regular Ca^{2+} site with inversion symmetry and charge compensation at large distance.

The photoluminescence decay of CaO:1at.%Eu (C, H_2/N_2) after 280 nm excitation is shown in Figure 6b. At an emission wavelength of 625 nm (Curve 1) the majority of the detected signal comes from the Eu^{3+} $4f^6[^5D_0] \rightarrow 4f^6[^7F_2]$ emission. The overlap of the Eu^{2+} $4f^65d \rightarrow 4f^7$ emission with the Eu^{3+} $4f^6[^5D_0] \rightarrow 4f^6[^7F_2]$ emission (Figure 5c) is visible as fast component with about 1 μs decay time. After about 10 μs, the signal from Eu^{2+} has decayed enough that the decay curve becomes representative for the luminescence decay of Eu^{3+}. Opposed to the Eu^{3+} emission in CaO:1at.%Eu (air), the decay curve in CaO:1at.%Eu (C, H_2/N_2) is severely non-exponential. After the first 50 μs, the decay converges to a component with decay time of 140 μs, almost ten times faster than the 1.3 ms decay time observed in CaO:1at.%Eu (air). This much shorter decay time is another indication of radiationless energy transfer from Eu^{3+} to Eu^{2+}.

At an emission wavelength of 800 nm (Curve 2), the Eu^{2+} $4f^65d \rightarrow 4f^7$ emission is monitored. The first 10 μs of the decay curve are dominated by a fast component with a 900 ns decay time, which matches well with the intrinsic decay time of the Eu^{2+} $4f^65d \rightarrow 4f^7$ emission.[17] After 10 μs, a slow component becomes visible that decays at the same rate as the Eu^{3+} decay curve (Curve 1). This slow component originates from the $4f^65d \rightarrow 4f^7$ emission after Eu^{2+} is excited through energy transfer from Eu^{3+}.

3. Discussion

A primary condition for energy transfer from Eu^{3+} to Eu^{2+} is that the excitation bands of Eu^{2+} overlap with the emission lines of Eu^{3+}. This requires that the Eu^{2+} emission lies beyond about 600 nm, i.e. close to the NIR part of the spectrum. It is shown schematically in **Figure 7**. On the left side of the figure is the situation for almost all known Eu^{2+}-Eu^{3+}-co-doped compounds, where the lowest Eu^{2+} $4f^65d$ state lies above the Eu^{3+} $4f^6[^5D_0]$ state. After Eu^{2+} gets excited through Arrow 1, its emission wavelength is short enough that after relaxation energy can be transferred to Eu^{3+} through Arrow 2. Eu^{3+} will then relax down to the $4f^6[^5D_0]$ state. There is not enough energy available to transfer its excitation back to Eu^{2+} from the Eu^{3+} $4f^6[^5D_0]$ state. Therefore, Eu^{3+} will show $4f^6 \rightarrow 4f^6$ emission from the $4f^6[^5D_0]$ state (Arrow 3). The situation in the left side of the figure is required for sensitization of the Eu^{3+} emission by Eu^{2+} as a co-dopant, resulting in white light emitting phosphors if energy transfer is not complete and the Eu^{2+} is in the blue-green part of the spectrum.[12,13] s CaO:Eu^{2+},Eu^{3+} is a phosphor for which the situation on the right side in Figure 7 applies. Here, the lowest Eu^{2+} $4f^65d$ state

**ADVANCED
SCIENCE NEWS**

www.advancedsciencenews.com

**ADVANCED
OPTICAL
MATERIALS**
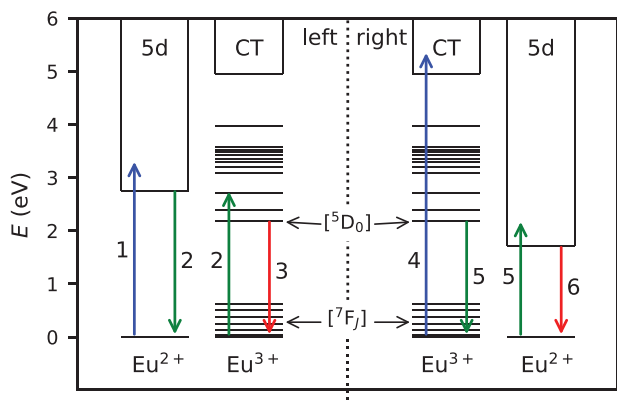
www.advopticalmat.de

Figure 7. Schematic showing energy transfer between Eu^{2+} and Eu^{3+}. Left: The lowest $4f^6 5d$ level of Eu^{2+} lies above the Eu^{3+} $4f^6[^5D_0]$ level and energy transfer occurs from Eu^{2+} to Eu^{3+}. Right: The lowest $4f^6 5d$ level of Eu^{2+} lies below the Eu^{3+} $4f^6[^5D_0]$ level and energy transfer occurs from Eu^{3+} to Eu^{2+}.

lies below the Eu^{3+} $4f^6[^5D_0]$ state. In this situation, when exciting Eu^{3+} through Arrow 4 in the CT state, first it will relax down to the $4f^6[^5D_0]$ state. Now, still enough energy is available to subsequently transfer its excitation energy to Eu^{2+} through Arrows 5, which will then relax down to the lowest $4f^6 5d$ state. Again, energy is lost in the relaxation process and transfer back to Eu^{3+} is no longer possible. Therefore, finally Eu^{2+} will show $4f^6 5d \rightarrow 4f^7$ emission through Arrow 6.

The efficiency of energy transfer η depends strongly on the oscillator strength of the acceptor ion.[16] The oscillator strength of the donor ion has no effect as long as energy transfer between donors is negligible.[52] As the oscillator strength of the Eu^{2+} $4f^7 \rightarrow 4f^6 5d$ transitions is about three orders of magnitude larger than that of the Eu^{3+} $4f^6 \rightarrow 4f^6$ transitions, energy transfer from Eu^{3+} to Eu^{2+} can be much more efficient than energy transfer from Eu^{2+} to Eu^{3+} for the same concentrations.

The energy transfer efficiency is typically calculated from the normalized luminescence decay curves of the donor ion with and without acceptor ions present in the sample.[53] These samples would in this case be CaO:1at.%Eu (C, H_2/N_2) and CaO:1at.%Eu (Air), respectively. In this case, however, decay curves of CaO:1at.%Eu are composed of the luminescence decay from multiple Eu^{3+} centers, each with their own decay time. It is likely that the presence of Eu^{2+} influences the ratio between different Eu^{3+} centers, or even causes the formation of new kinds of Eu^{3+} centers, as suggested by the Mössbauer data. This would in turn change the intrinsic luminescence decay of Eu^{3+} ions. The situation is further complicated by the overlap between the Eu^{3+} and Eu^{2+} emission spectra in CaO:1at.%Eu (C, H_2/N_2), meaning the Eu^{3+} decay cannot be measured without picking up signal from the Eu^{2+} decay (Figure 6). Because of this we use a simplified method and roughly estimate the $Eu^{3+} \rightarrow Eu^{2+}$ energy transfer efficiency (η) through Equation (1).

$$\eta = 1 - \frac{\tau_C}{\tau_{Air}} \qquad (1)$$

Here, τ_{Air} is the Eu^{3+} decay time of the CaO:1at.%Eu (Air) sample. A value of 1.3 ms is taken, corresponding to the primary com-

ponent. τ_C is the Eu^{3+} decay time of the CaO:1at.%Eu (C, H_2/N_2) sample. As the decay curve of CaO:1at.%Eu (C, H_2/N_2) is non-exponential, the slowest component of 140 µs is taken (Figure 6b). Equation (1) is a simplified version of the well-known formula derived by Inokuti and Hirayama,[53] where τ_{Air} and τ_C are replaced by the mean decay times of their respective decay curves. Using the decay times of the fastest component in the CaO:1at.%Eu (Air) sample and slowest component in the CaO:1at.%Eu (C, H_2/N_2) therefore results in a significant underestimation of the energy transfer efficiency. With these decay times a value of $\eta \approx 90\%$ is found, indicating that most of the excitations from Eu^{3+} are transferred to Eu^{2+}. This is also in line with the photoluminescence emission spectrum of CaO:1at.%Eu (C, H_2/N_2) in Figure 5c, where upon excitation in the Eu^{3+} CT band, over 95% of the emission spectrum consists of Eu^{2+} $4f^6 5d \rightarrow 4f^7$ emission.

In phosphors where energy transfer from Eu^{2+} to Eu^{3+} is possible, the internal quantum efficiency of the Eu^{2+} emission degrades with increasing Eu^{3+} concentration.[54] As in CaO the Eu^{2+} $4f^6 5d \rightarrow 4f^7$ transition lies at longer wavelength than the Eu^{3+} $4f^6[^7F_0] \rightarrow 4f^6[^5D_0]$ transition, the energy transfer is in the opposite direction. Therefore, it is no longer necessary to reduce all Eu^{3+} to Eu^{2+} to attain high internal quantum efficiency of the Eu^{2+} emission. In many cases, the decay time of the Eu^{2+} emission can be directly linked to its quantum efficiency, i.e., the quantum efficiency is high for slow decay. The decay curve of the Eu^{2+} emission in CaO:Eu^{2+},Eu^{3+} reported in literature for varying Eu^{3+} concentrations is often well approximated by a single exponential with 1 µs decay time,[17,18] in accordance with the decay time of Eu^{2+} measured in this work. This means that once Eu^{2+} is in the excited state, the probability of emission is similar in all samples, i.e., the Eu^{2+} is not quenched by presence of Eu^{3+}. Additionally, when the ratio of Eu^{3+} to Eu^{2+} is high, using a UV-blue pump LED may result in some Eu^{3+} excitation through the many $4f^6 \rightarrow 4f^6$ transitions in that wavelength region. As $Eu^{3+} \rightarrow Eu^{2+}$ energy transfer can also be efficient at low Eu^{2+} concentrations, these excitations will still result in Eu^{2+} emission. From this can be learned that full reduction of Eu^{3+} to Eu^{2+} is not necessary for Eu^{2+}-doped NIR LED phosphors.

Qiao et al. reported a high internal quantum efficiency of about 76% for CaO:Eu^{2+},Eu^{3+} despite a significant amount of Eu^{3+} considered as a killer center still being present in their samples.[18] However, from our work it has become clear that Eu^{3+} does not act as a killer center for the Eu^{2+} emission in CaO:Eu^{2+},Eu^{3+}, due to $Eu^{3+} \rightarrow Eu^{2+}$ energy transfer. Moreover, the internal quantum efficiency reported in ref. [18] is much higher than the 20% of the CaO:1at.%Eu (C, H_2/N_2) sample measured in this work. As the Eu^{2+} emission is not quenched, it must be concluded that the difference in internal quantum efficiency is caused by a process that occurs before Eu^{2+} gets excited. This suggests that there is parasitic absorption that does not result in luminescence. Such parasitic absorption may be caused by impurities in the starting materials, defects introduced by reducing conditions during synthesis (e.g., O^{2-} vacancies), heat treatment (e.g., F-centers), or mechanical stress due to milling.[33,34] It has indeed been demonstrated that many such defects will lead to additional absorption bands.[32] This suggests that the most effective way to increase quantum efficiency of the Eu^{2+} emission of a CaO:Eu phosphor is to reduce the number of impurities and defects in the host compound. This can be achieved by minimizing mechanical stress

**ADVANCED
SCIENCE NEWS**

www.advancedsciencenews.com

**ADVANCED
OPTICAL
MATERIALS**

www.advopticalmat.de

and annealing the samples, or using flux agents that prevent sintering of the reaction product. Additionally, increasing the Eu concentration would help to increase the probability that an incoming photon is absorbed by Eu instead of an impurity or defect. Due to the poor solubility of Eu^{3+} in the CaO host, a higher Eu concentration can potentially be achieved by using Eu(II)O as a starting compound instead of $Eu(III)_2O_3$.

For the development of NIR LEDs, there may be a desire to shift the Eu^{2+} $4f^65d \rightarrow 4f^7$ emission to longer wavelengths than the 720 nm in CaO:Eu. Longer emission wavelength can often be achieved by increasing the crystal field strength around Eu^{2+}, which in turn can be achieved by reducing the ionic radius of the host cation. For example in CaO, replacing part of Ca^{2+} by Mg^{2+}, resulting in $Ca_{1-x}Mg_xO$ solid solutions. Due to the smaller size of Mg^{2+}, the solubility of Eu^{2+} (which is larger than Ca^{2+}), is expected to decrease. This effect and the similar ionic radii of Eu^{3+} and Ca^{2+} will result in a relatively higher Eu^{3+} content. However, due to the efficient energy transfer from Eu^{3+} to Eu^{2+}, this does not have to pose any problem for application.

Replacing the O^{2-} anion by S^{2-} or Se^{2-} to increase the nephelauxetic effect does not result in a longer Eu^{2+} $4f^65d \rightarrow 4f^7$ emission wavelength in compounds with the rock salt structure. In CaS for example, the Eu^{2+} emission maximum lies at 650 nm and when going to CaSe the Eu^{2+} emission maximum is at an even shorter wavelength of 600 nm.[55] While the increased nephelauxetic effect decreases the energy of the barycenter of the $4f^65d$ excitation bands, the replacement of O^{2-} by the larger S^{2-} or Se^{2-} anions reduces the crystal field strength, which results in less splitting of the $4f^65d$ excitation bands. The combined effect is that the lowest $4f^65d$ level shifts to higher energy, i.e., shorter wavelength. Another route to achieve a larger nephelauxetic effect is the partial replacement of O^{2-} by N^{3-}. Due to the smaller ionic radius of N^{3-} compared to S^{2-}, this route likely does not decrease the crystal field strength as much and is expected to result in longer wavelength Eu^{2+} emission. N^{3-} replacing O^{2-} however requires charge compensation, which can be introduced in the form of Y^{3+} replacing Ca^{2+}. The presence of Y^{3+} ions may increase the relative Eu^{3+} concentration. Again, the presence of only about 0.3–0.4 at.% Eu^{2+} might be enough to completely eliminate this problem of a higher Eu^{3+} concentration, as energy is efficiently transferred from Eu^{3+} to Eu^{2+} for NIR Eu^{2+} emission.

4. Conclusion

In this work, the Eu^{2+} concentration in CaO:1at.%Eu has been increased by means of adding graphite powder to the starting materials and heating the starting mixture in an H_2/N_2 atmosphere. The increase in Eu^{2+} concentration was confirmed through X-ray diffraction, Eu Mössbauer spectroscopy, and optical absorption measurements and estimated to be approximately 0.3–0.4 at.%. Using CaO:Eu^{2+},Eu^{3+} as a model compound, energy transfer from Eu^{3+} to Eu^{2+} has been demonstrated for the first time. Such energy transfer is possible because the lowest Eu^{2+} $4f^65d$ band lies at a lower energy (13900 cm^{-1}, about 720 nm) than the Eu^{3+} $4f^6[^5D_0]$ level. This means that the quantum efficiency of the Eu^{2+} emission does not degrade upon the increase of the Eu^{3+} concentration, i.e., Eu^{3+} does not act as a killer center for NIR Eu^{2+} emission in contrast to UV–vis Eu^{2+} emission. As a consequence, it is not required to reduce all Eu^{3+} to Eu^{2+} for obtaining

high quantum efficiency of the Eu^{2+} emission. Instead, it is essential to avoid parasitic absorption due to impurities and defects, e.g., as a consequence of mechanical stress. Even at dopant concentrations concentrations of only about 0.3–0.4 at.% Eu^{2+}, the energy transfer efficiency is high (> 90%), owing to the high oscillator strength of the $4f^7 \rightarrow 4f^65d$ excitation transition of the Eu^{2+} acceptor ion. The discovery of such efficient $Eu^{3+} \rightarrow Eu^{2+}$ energy transfer may pave the way for developing new strategies for improvement of mixed valency Eu-doped phosphors, with long wavelength Eu^{2+} emission for application in NIR LEDs.

5. Experimental Section

Three samples of CaO:1at.%Eu were synthesized through a solid-state reaction, meaning that 1at.% of the Ca^{2+} ions were replaced by Eu^{3+} in the mixture of starting materials. Stoichiometric amounts of $CaCO_3$ (Merck, 2N) and Eu_2O_3 (Aldrich, 4N) were mixed and ground in a mortar and pestle. The mixture of starting materials was placed in an alumina crucible and heated inside a tube furnace to 1200 °C for 10 h. At this temperature $CaCO_3$ decomposes into CaO and CO_2 according to:

$$CaCO_3 \rightarrow CaO + CO_2 \tag{2}$$

During the heating process, Eu was incorporated as a dopant in the CaO host lattice. Three different synthesis methods were applied. One sample was synthesized in static air. The second sample was synthesized in a flowing atmosphere of 7 vol.% H_2 and 93 vol.% N_2 (H_2/N_2) to help reduce Eu^{3+} in the $Eu(III)_2O_3$ starting material to Eu^{2+}. The last sample was also synthesized in an H_2/N_2 atmosphere and in addition graphite powder was added as a reducing agent by mixing with the powder mixture in a stoichiometric ratio. In H_2/N_2 atmosphere, the conversion of Eu^{3+} (in the raw material $Eu(III)_2O_3$) into Eu^{2+} was taking place according to the reaction:

$$Eu(III)_2O_3 + H_2 \rightarrow 2Eu(II)O + H_2O \tag{3}$$

When adding C and heating in H_2/N_2 atmosphere, the additional reduction of Eu^{3+} would take place by the reaction:

$$Eu(III)_2O_3 + C \rightarrow 2Eu(II)O + CO \tag{4}$$

There was also an attempt to use Ca_3N_2 in an H_2/N_2 atmosphere as an agent to reduce Eu^{3+}, in a similar way as Si_3N_4 was effective for this purpose.[30,31] The expected reaction equation is:

$$3Eu(III)_2O_3 + Ca_3N_2 \rightarrow 6Eu(II)O + 3CaO + N_2 \tag{5}$$
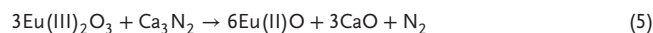
According to this reaction equation, in the ideal case a solid solution $Ca_{0.333}Eu(II)_{0.667}O$ with cubic rocksalt structure was formed. However, the results obtained with this synthesis method were not conclusive with respect to the increase of the Eu^{2+} concentration, so possibly instead N^{3-} on the O^{2-} site was used as charge compensator for the replacement of Ca^{2+} by Eu^{3+}. Therefore, this synthesis route was not pursued anymore.

To study the effects of Eu-doping on the lattice parameters and optical absorption, one sample of undoped CaO was prepared by heating only $CaCO_3$ to 1200 °C for 10 h in air. All reaction products were slightly sintered and had to be lightly ground to a powder. Care was taken to minimize the mechanical stress during this process, as this is known to cause luminescent defects in CaO.[32–34] Since the samples were sensitive to reaction with CO_2 and H_2O, storage and handling was done in a nitrogen filled glovebox (H_2O < 0.1 ppm) and airtight sample holders.

X-ray diffractograms were recorded using a PANalytical Xpert Pro MPD diffractometer with copper anode. An X-ray tube voltage of 45 kV and current of 40 mA were used. The measurements were performed with a stepsize of 0.002° and 0.08 s counting time per step. The samples were

contained in airtight sample holders covered with Kapton foil. For the determination of the cubic lattice parameter a, Si was used as an internal standard. As CaO and Si are both cubic lattices, a can be calculated for each individual diffraction peak. Systematic errors in θ caused by small offsets in sample placement have been minimized by plotting a versus the function $f(\theta)$ and extrapolating to: $f(\theta) = 0$:[35]

$$f(\theta) = \frac{\cos^2(\theta)}{\sin(\theta)} + \frac{\cos^2(\theta)}{\theta} \qquad (6)$$

Kubelka–Munk absorption spectra were measured using a Bruker Vertex 80V Fourier transform spectrometer, using a W lamp as light source and Si photodetector. The semi-infinite thick samples were contained in identical airtight sample holders with fused silica window, which were mounted on a Pike EasiDiff diffuse reflection accessory. The specular reflection from the sample holder window was blocked by a beam blocker at the exit of the sample chamber. A sample holder containing undoped CaO was used as reference.

Transmission ^{151}Eu Mössbauer spectra were collected at room temperature with a conventional constant-acceleration spectrometer using a ^{151}SmF$_3$ source. Velocity calibration was carried out using a Fe$_2$O$_3$ absorber and a ^{57}Co source. The isomer shift values were reported relative to EuF$_3$ as a reference sample. The Mössbauer spectra were fitted with Lorentzian functions using the Mosswinn 4.0 program.[36]

Photoluminescence excitation and emission spectra were recorded using a 450 W Xenon lamp combined with a Horiba Gemini 180 monochromator as the excitation source. The light coming from the sample passed through an optical filter to remove the excitation light from the spectrum before passing through a Princeton Instruments SpectraPro SP2358 monochromator. The light was then detected by a Hamamatsu R7600-20 PMT.

Internal quantum efficiency measurements were performed using a Thorlabs M470L3 LED emitting at 470 nm as excitation source. The sample was contained in a white sample holder with fused silica window and placed inside a Labsphere integrating sphere. The light from inside the sphere was coupled into an optical fiber and detected using an Ocean Insight QEPro spectrometer. A sample holder containing undoped CaO was used as a reference.

Photoluminescence decay curves and time-gated emission spectra were measured using an EKSPLA NT230 OPO laser to excite the sample. The emission of the sample passed through a Princeton Instruments SpectraPro-SP2358 monochromator before being detected by a Hamamatsu R7600-U-20 PMT. An optical filter was placed in front of the monochromator to filter out the excitation light of the laser. The signal from the PMT was recorded using a CAEN DT5724F digitizer.

Conflict of Interest

The authors declare no conflict of interest.

Data Availability Statement

The data that support the findings of this study are available from the corresponding author upon reasonable request.

[1] G. Blasse, A. Bril, W. C. Nieuwpoort, *J. Phys. Chem. Solids* **1966**, *27*, 1587.

[2] G. Blasse, B. C. Grabmaier, *Luminescent Materials*, Springer-Verlag, Berlin **1994**.

[3] Z. Tang, Q. Zhang, Y. Cao, Y. Li, Y. Wang, *Chem. Eng. J.* **2020**, *388*, 124231.

[4] B. M. J. Smets, *Mat. Chem. Phys.* **1987**, *16*, 283.

[5] S. Adachi, *ECS J. Solid State Sci. Technol.* **2023**, *12*, 016002.

[6] J. Qiao, G. Zhou, Y. Zhou, Q. Zhang, Z. Xia, *Nat. Commun.* **2019**, *10*, 5267.

[7] J. Liang, P. Du, H. Guo, L. Sun, B. Li, X. Huang, *Dyes Pigm.* **2018**, *157*, 40.

[8] M. A. van de Haar, J. Werner, N. Kratz, T. Hilgerink, M. Tachikirt J. Honold, M. R. Krames, *Appl. Phys. Lett.* **2018**, *112*, 132101.

[9] M. A. van de Haar, A. C. Berends, M. R. Krames, L. Chepyga, F. T. Rabouw, A. Meijerink, *J. Phys. Chem. Lett.* **2020**, *11*, 689.

[10] W. Chen, Y. Ouyang, M. Mo, H. Zhang, Q. Su, *J. Lum.* **2021**, *229*, 117672.

[11] W. B. Dai, *J. Mat. Chem. C* **2014**, *2*, 3951.

[12] X. Gao, H. Liu, X. Yang, Y. Tian, X. Lua, L. Han, *RSC Adv.* **2017**, *7*, 1711.

[13] R. Yu, J. Wang, Z. Zhao, M. Li, S. Huo, J. Li, J. Wang, *Mater. Lett.* **2015**, *160*, 294.

[14] Z. Wang, H. Fu, X. Zhan, B. Tong, G. Ma, H. T. Hintzen, *J. Rare Earths*, (in press) **2023**.

[15] Th. Förster, *Ann. Phys.* **1948**, *437*, 55.

[16] D. L. Dexter, *J. Chem. Phys.* **1953**, *21*, 836.

[17] N. Yamashita, *J. Electrochem. Soc.* **1993**, *140*, 840.

[18] J. Qiao, S. Zhang, X. Zhou, W. Chen, R. Gautier, Z. Xia, *Adv. Mater.* **2022**, *34*, 2201887.

[19] Q. Zhao, Y. Wang, T. Duan, F. Xie, H. Zou, Y. Song, Y. Sheng, *J. Lumin.* **2023**, *253*, 119457.

[20] Z. Hao, Y. Wang, L. Zhang, G. Pan, X. Zhang, H. Wu, Y. Luo, J. Zhang, *Opt. Mater.* **2017**, *71*, 1.

[21] R. Zhou, J. Li, Y. Huang, B. Liu, D. Hua, J. Zhou, T. Deng, Q. Li, J. Li, H. Zhao, *J. All. and Comp.* **2023**, *940*, 168706.

[22] X. Lu, J. Ma, H. Li, F. Zhang, Z. Jin, W. Xie, *ECS J. Sol. State Sci. and Techn.* **2022**, *11*, 086001.

[23] C. W. Yeh, W. T. Chen, R. S. Liu, S. F. Hu, H. S. Sheu, J. M. Chen, H. T. Hintzen, *J. Am. Chem. Soc.* **2012**, *134*, 14108.

[24] L. Amidani, K. Korthout, J. J. Joos, M. van der Linden, H. F. Sijbom, A. Meijerink, D. Poelman, P. F. Smet, P. Glatzel, *Chem. Mat.* **2017**, *29*, 10122.

[25] D. de Graaf, H. T. Hintzen, G. de With, K. V. Ramanujachary, C. Lanci, S. E. Lofland, *Sol. State Comm.* **2004**, *131*, 693.

[26] F. Steudel, J. A. Johnson, C. E. Johnson, S. Schweizer, *Materials* **2018**, *11*, 828.

[27] H. T. Hintzen, H. M. van Noort, *J. Phys. Chem. Sol.* **1988**, *49*, 873.

[28] P. Boolchand, K. C. Mishra, M. Raukas, A. Ellens, P. C. Schmidt, *Phys. Rev. B* **2002**, *66*, 134429.

[29] H. T. Hintzen, C. J. M. Denissen, H. M. van Noort, *Mat. Res. Bull* **1989**, *24*, 247.

[30] D. de Graaf, H. T. Hintzen, S. Hampshire, G. de With, *J. Eur. Ceram. Soc., J. Eur. Ceram. Soc.* **2003**, *23*, 1093.

**ADVANCED
SCIENCE NEWS**

www.advancedsciencenews.com

**ADVANCED
OPTICAL
MATERIALS**

www.advopticalmat.de

[31] H. T. Hintzen, J. W. H. van Krevel, D. de Graaf, R. Metselaar, Y. Menke, S. Hampshire, *J. Mat. Sci.* **2004**, *39*, 2237.

[32] P. M. Jaffe, *J. Electrochem. Soc.* **1962**, *109*, 872.

[33] Y. Chen, M. M. Abraham, T. J. Turner, C. M. Nelson, *Philos. Mag.* **1975**, *32*, 99.

[34] A. Remón, J. Piqueras, *Cryst. Res. Technol.* **1985**, *20*, 582.

[35] B. D. Cullity, *Elements of X-ray Diffraction*, 2nd ed., Addison-Wesley Publishing Company Inc., London **1978**, pp. 352–358.

[36] Z. Klencsár, *Nucl. Instr. Meth. B* **1997**, *129*, 527.

[37] Q. Zhao, B. Qian, Y. Wang, T. Duan, H. Zou, Y. Song, Y. Sheng, *J. Lumin.* **2022**, *241*, 118491.

[38] D. R. Black, D. Windover, A. Henins, D. Gil, J. Filliben, J. P. Cline, *Powder Diffr.* **2010**, *25*, 187.

[39] D. Taylor, *Brit. Ceram. Trans. J.* **1984**, *83*, 5.

[40] H. T. Hintzen, H. A. M. van Hal, C. Langereis, C. J. M. Denissen, *J. Less-Common Met.* **1989**, *155*, 291.

[41] D. van der Voort, A. Imhof, G. Blasse, *J. Solid State Chem.* **1992**, *96*, 311.

[42] S. Kumar, G. N. Rao, O. K. Medhi, U. Agarwala, *Z. Naturforsch* **1974**, *29*, 1778.

[43] M. Pham-Thi, N. Ruelle, E. Tronc, D. Simons, D. Vivien, *Jpn. J. Appl. Phys.* **1994**, *33*, 1876.

[44] C. E. Johnson, L. Costa, J. A. Johnson, D. E. Brown, S. Somarajan, W. He, J. H. Dickerson, *J. Phys. D Appl. Phys.* **2014**, *47*, 75001.

[45] M. Zeuner, S. Pagano, P. Matthes, D. Bichler, D. Johrendt, T. Harmening, R. Pöttgen, W. Schnick, *J. Am. Chem. Soc.* **2009**, *131*, 11242.

[46] H. A. Höppe, H. Trill, B. D. Mosel, H. Eckert, G. Kotzyba, R. Pöttgen, W. Schnick, *J. Phys. Chem. Solids* **2002**, *63*, 853.

[47] R. Pöttgen, O. Reckeweg, *Z. Kristallogr.* **2017**, *232*, 653.

[48] L. C. Porter, J. C. Wright, *J. Chem. Phys.* **1982**, *77*, 2322.

[49] B. Bihari, H. Eilers, B. M. Tissue, *J. Lumin.* **1997**, *75*, 1.

[50] W. Chen, A. G. Joly, C. M. Kowalchuk, J.-O. Malm, Y. Huang, J.-O. Bovin, *J. Phys. Chem. B* **2002**, *107*, 7034.

[51] J. Zheng, C. Liu, H. Yu, L. Chen, M. Yang, H. Zhao, B. Lu, F. Yang, H. Feng, *Cryst. Res. Techn.* **2022**, *57*, 2100120.

[52] A. I. Burshteĭn, *Sov. Phys. Uspekhi* **1984**, *27*, 579.

[53] M. Inokuti, F. Hirayama, *J. Chem. Phys.* **1965**, *43*, 1978.

[54] S. Li, L. Wang, D. Tang, Y. Cho, X. Liu, X. Zhou, L. Lu, L. Zhang, T. Takeda, N. Hirosaki, R.-J. Xie, *Chem Mater.* **2018**, *30*, 494.

[55] N. Yamashita, O. Harada, K. Nakamura, *Jpn. J. Appl. Phys.* **1995**, *34*, 5539.